RACER – TESTING OF MAJOR COMPONENTS

Martin Blacha, Airbus Helicopters, Donauwörth, Germany
Peter Burden, Hamble Aerostructures, Hamble, United Kingdom

Abstract

In the frame of the European Clean Sky 2 initiative the RACER, as a demonstrator for high-speed rotorcraft transport, is developed at Airbus Helicopters in co-operation with multiple research, development, and manufacturing partners all over Europe. As a new rotorcraft concept with new structural design principles structural testing is required to support the demonstration of airworthiness. Due to the contribution from independent partners and multiple constraints an appropriate test campaign based upon separated tests had to be performed. This testing campaign specifically follows two major aspects: At first to demonstrate that the structural components can take limit loads occurring during flight and ground operation, and second, to demonstrate that the new concept of the RACER including all related design principles are well reflected and represented in the analysis models used for substantiation. Both aspects and their outcomes are considered in this paper and in the absence of a full airframe dedicated for testing, the general testing philosophy for the RACER is described.

1. NOTATION

Acronyms:	
CS	Certification Specification
DVI	Direct Visible Inspection
ERF	European Rotorcraft Forum
FE	Finite Element
GFEM	Global Finite Element Model
LDL	Lateral Drive Line (drive shaft)
LFEC	Low Frequency Eddie Current
LH	Left hand
LL	Limit Load
LRGB	Lateral Gear Box
LVDT	Linear Variable Displacement Transducers
MGB	Main Gear Box
MTOW	Maximum Take Off Weight
PtF	Permit to Flight
RACER	Rapid And Clean European Rotorcraft
RH	Right hand
SDI	Special detailed Inspection (NDT required)
SLP	Single load path
UL	Ultimate Load
VFS	Vertical Flight Society

2. INTRODUCTION

The RACER is a European rotorcraft demonstrator designed and manufactured by numerous European companies, research institutes, and universities in the frame of the CleanSky2 activities of the European Union. This consortium is technically led by Airbus Helicopters. As the design organization, Airbus is also responsible for the definition and coordination of all activities for demonstrating airworthiness in order to achieve the permit to fly (PtF).

As the RACER's conceptual design has several major design principles new to helicopters, demonstrating airworthiness requires testing. Due to the RACER's MTOW it is a CS29 (Ref. 1) rotorcraft and although the approval is PtF, it must comply with CS29 airworthiness regulations

As mentioned above, the RACER's design is new in major design features. This implies that the internal load distribution of some forces applied to the structure has no preceding example that Airbus has experience with. Thus the test campaign has to prove that the global load distribution in the real vehicle is as predicted. This means that the test campaign which is based upon the common test pyramid (see Ref. 2) has to include a test which proves the validity of the models used for the global load distribution and substantiation.

In the frame of this research project it was not foreseen to build a dedicated full-scale airframe as a static test specimen. An alternative solution was structural testing on the flying demonstrator itself but the risk of damage to the flying prototype was considered too high. Consequently a hybrid strategy was chosen: For proving structural strength, tests were carried out at sub-assembly level for major components or new design principles. For the justification of the global model, simple generic tests on the flying demonstrator were performed. Element and coupon tests for the characterization of new materials and/or processes were conducted. Thorough test campaigns for bird strike, the dynamic system, flight controls and other systems were also conducted.

This paper focusses on the description of the main structural tests of the airframe.

3. Basic information on the RACER and main test purpose

3.1. The RACER's architecture

The unique configuration of the RACER with its characteristic design features and the resulting technical challenges have been described in various previous publications, for example in Ref. 3 to Ref. 10. A detailed in-sight of the main structural components and their arrangement is provided in Ref. 4 hence this paper gives a brief overview only. Figure 1 shows the RACER as a compound rotorcraft with the joined wing as the most obvious and characteristic feature.

Figure 1: The RACER as a demonstrator of high-speed compound rotorcraft.

As the wings generate lift in forward flight and accommodate the lateral rotors at each wing tip they are significantly loaded by both aerodynamic forces and the forces and moments generated by the lateral rotors. In contrast to mono-wings such as the RACER's predecessor X³, the wings are attached to the upper deck of the fuselage and to the bottom of the fuselage. In order to cope with these forces, the design principles in these regions of the fuselage are different: The mechanical deck comprises cross-beams for the interconnection of the upper wings and the bottom fuselage features a stub-wing attaching the lower wing and the main landing gear. As a consequence both regions comprise new design principles compared to conventional helicopters, see Ref. 4.

Figure 2 and Figure 3 show these two regions on the helicopter.

Figure 2: The mechanical deck of the RACER at the upper wing root with its main structural arrangement including frame 3, frame 4, the cross-beams, and the engine deck.

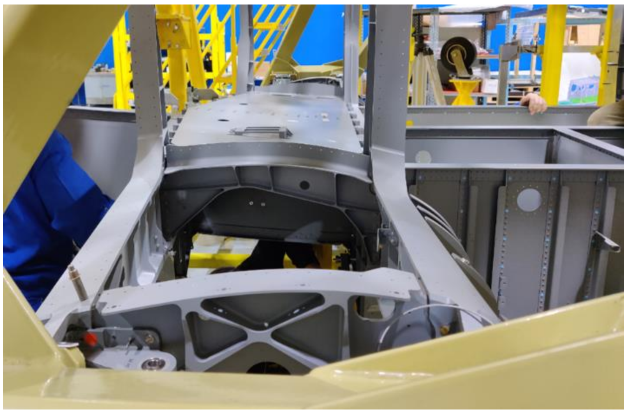

Figure 3: The stub wing region at the lower wing connection to the fuselage, with frame 4 and 5, root and end ribs (by courtesy of the Romanian consortium RoRcraft).

The joined wings themselves are also newly developed items with important functions and thus they too are in the main scope of structural testing.

3.2. Permit to fly strategy for the demonstrator

In contrast to the development of a completely new serial helicopter the RACER is a demonstrator only. This helicopter has a limited in-service time with limited amount of flight hours in a controlled environment and under permanent surveillance, continuous check of the main systems and a stepwise opening of the flight envelope. All this reduces the amount of required testing which was already introduced in Ref. 4.

The main aspects of testing as highlighted in Ref. 4 can be summarized as follows:

1) Proof of structural strength testing up to limit load (ultimate load capability shown by analysis).
2) For the uppermost levels of the test pyramid (see §4) separate sub-component test specimen are built with identical material, geometry, and manufacturing processes.
3) No complete full scale airframe is built, instead separate sub-component tests are built (see next chapter).
4) Without complete structural representation of the full vehicle for the static tests, the accuracy of the model used for load distribution has to be shown in a global airframe test as well (application of unit loads on the flying vehicle).
5) The strategy to use separate test specimen reduces the risk of damaging the flying demonstrator.

It is important to highlight that for the analysis activities accompanying the tests only approved methods and tools have been used, proven with past experience. In the next chapter the strategy for the main structural tests will be detailed.

4. General strategy for structural testing

The RACER is a demonstrator only but for future missions and serial production the goal is for RACER to be certifiable based upon CS 29 paragraphs (see Ref. 1). Accordingly, the PtF activities were based upon the requirements defined in these paragraphs. Despite the possible simplifications and reliefs for PtF (see previous chapter), the complete test strategy is based upon the common test pyramid as defined in Ref. 2.

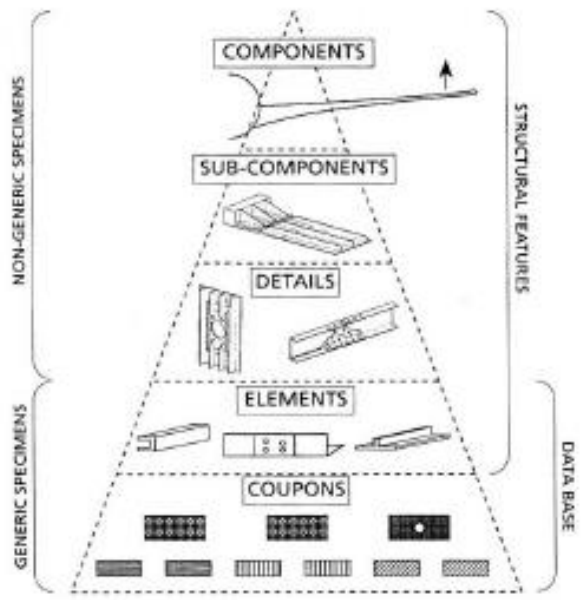

Figure 4: Test pyramid as defined in Ref. 2.

The decision to split up the structural test campaign of the RACER was necessary for several reasons. The main airframe was developed in co-operation with numerous European partners with different development schedules thus necessitating separate sub-component tests.

In order to prove the separation strategy is valid at helicopter level a dedicated GFEM-correctness test will be performed on the real flying prototype with unitary loads well below LL. These load cases are simple, unitary and basically artificial loading conditions. The intention of creating clear and distinct loading conditions is to verify their respective load paths through the structure, in turn simplifying the interpretation and evaluation of the test results.

One of these simple unitary loadings is shown as example in Figure 5. The figure shows a vertical load applied to the RH wing tip by a platform loaded with sand-bags (in orange). The platform is connected to the wing tip by a rope and a beam which curves around the structure blocking the vertical direction. The same load was applied simultaneously on the LH wing tip so that a symmetric wing load case with single forces was created. This arrangement was then changed to an asymmetric load case with single loads pointing up on one wing and down on the opposite wing or in forward and aft direction respectively.

Figure 5: Example for the GFEM accuracy test on the flying demonstrator with loads applied by sand bags (in orange) at the wing tips.

These tests on the real flying prototype validate the predictability of the GFEM in a simple manner: If the different sub-component tests correlate with the predictions made on the basis of the GFEM, it can be concluded that the global behavior of the model is representative. This would verify that the separate sub-component test strategy is valid as the global model is predictive.

The separate tests at sub-component level are described in the following chapters.

5. TESTING OF MAJOR COMPONENTS

5.1. Overview

As highlighted above, the RACER will fly for a limited amount of time only and will be inspected thoroughly with short inspection intervals during the flight test campaign. Moreover, a good data basis for the fatigue loads is available from the flight test campaign of the RACER's predecessor X³. This supported the decision to focus on static testing and reduce fatigue testing as much as possible. Only for items with a new manufacturing process used as PSEs application simplified fatigue tests were carried out.

As already mentioned, the main new design principles are located in the center fuselage. There are also new design features and manufacturing processes introduced in the tail boom. However, apart from the absence of a tail-rotor the function of the RACER's tail boom is mostly un-changed compared to conventional helicopters. Everything related to the load paths themselves are designed according to the common Airbus Helicopter design principles. Thus it was decided to separate the test campaign of the tail from the testing activities of the fuselage. The testing activities on the RACER's tail parts are published in Ref. 12 and thus not in the scope of this paper.

In Figure 6 an overview over the locations of the three main structural tests in the airframe are given. All new structural design principals of the RACER are located in the blue zone:

1) The stub wing area where the lower wings are attached to the fuselage and the main landing gear is retracted in a fixed-wing like manner (green zone in Figure 6). The testing in this area will be detailed in §5.2.
2) The upper deck area with the attachment of the upper wings (yellow zone in Figure 6). The testing in this area will be detailed in §5.3.
3) The wings including attachment of the lateral gear boxes. This area will be detailed in §5.4.

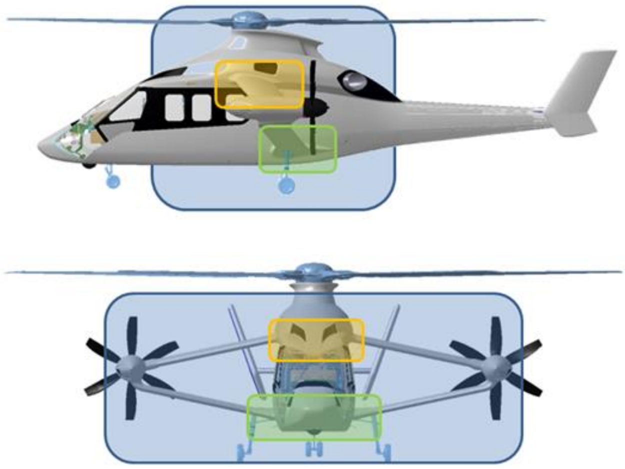

Figure 6: Overview of the main structural tests of the RACER's airframe and the main areas of interest.

5.2. Testing of the stub wing area

Set-up description:

As a consequence of the joined wing arrangement (staggered in the longitudinal direction of the vehicle), the fuselage experiences a comparatively complex superposition of vertical and longitudinal loads as well as bending and torsional moments. This results in a torsion of the center fuselage around its vertical and horizontal axis. The following figure gives an impression of this elastic movement for one flight load case in exaggerated view.

Figure 7: Elastic deformations of the fuselage under complex loading conditions in a front view (dynamic system and secondary structure not shown).

The asymmetry of loading and the resulting deformations drove the decision to consider the complete lower area of the fuselage as a representative specimen instead of reducing the specimen to one side only with symmetry at the center line. In addition to the flight loads occurring in this area the landing gear with its high interface loads is attached to the stub wing as well. In consequence this sub-component test was taken for testing of the flight load cases (wing related) and ground load cases (landing gear related). This test specimen and its fixation to the test rig is shown in Figure 8.

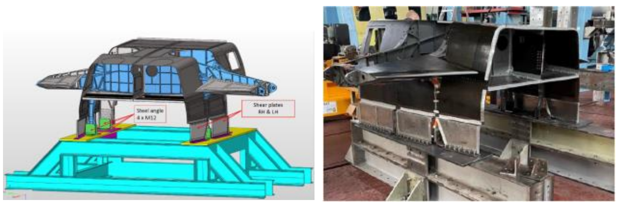

Figure 8: Stub-wing specimen as separated test set-up, courtesy of INCAS & AVIATEST.

The figure above shows that the specimen was turned upside down and fixed at its bottom end rigidly to the test support structure, see the large steel channel sections in the figure above. This arrangement provides sufficient space for the load application at the outer ends of the stub-wing and the main attachment points of the landing gear and simplifies measurements. In parallel an FE-model was built in order to support the test prediction on one hand and to prove the validity of the models used for the substantiation.

Test execution:

A general overview of the integration of the specimen into the test rig is given in Figure 9. The hydraulic cylinders shown in this figure act at the main load introduction points of the lower wing which represent the loads acting from the lower wing to the stub-wing. The example shows a rather symmetric loading scenario of LHS and RHS wing to the lower fuselage.

Figure 9: Basic arrangement of the stub-wing specimen in the test-rig for the wing load cases, courtesy of INCAS & AVIATEST.

The two sizing load cases (in flight and on ground) act during different flight phases: During flight the forces and moments of the lateral rotors are levered by the wingspan to the stub-wing attachment points, whereas the loads from the landing gear occur on ground where the forces of the lateral rotors are comparatively low. However, the load introduction points of stub-wing and main landing gear are in close proximity and locally act on the same main structural items. But these forces have different directions: the flight wing loads mainly act horizontally in contrast to the landing gear loads on ground acting vertically. Consequently the test campaign was split into separate sub-tests for flight and ground loading. This simplified sequential loading was proven to be valid by the corresponding simulations at GFEM-level. The limited superposition effect was covered by load enhancement factors for the sequential load application.

For one of the sizing wing load cases Figure 10 shows two actuators installed at the outer end of the stub wing which simulate the spanwise forces of the lower wing. For the measurement of displacements, a second independent rig was built up in order to de-couple the loaded specimen from the displacement transducers. This second rig consists of the light grey rods surrounding the stub-wing, see Figure 10.

Figure 10: Actuators simulating the wing loads on the RH stub-wing, courtesy of INCAS & AVIATEST.

As described above, dependent on the flight conditions the wings impose either symmetric or almost asymmetric loads to the fuselage. Hence there is a big variety of load cases in dedicated areas of the stub-wing: different propeller thrust cases in superposition with aerodynamic loads and accelerations for example. The extreme combinations of these load superpositions have been tested which enveloped all possible loading conditions. In Figure 11, an example is given about the different load vectors of the LH lower wing acting on the stub-wing at front and aft spar.

Figure 11: Actuators simulating the wing loads on the LH stub-wing, courtesy of INCAS & AVIATEST.

In comparison to Figure 10 it can be seen that the interface load vectors can differ extremely between both sides of the aircraft. It is to be pointed out that some of the cylinders act in tension, while others might be in compression.

In the next step of the test program the challenging loads resulting from the MLG during landing and ground operation were applied. A dummy landing gear was installed on the stub wing which simulates the wheel loads at the contact point wheel-to-ground. This dummy is the almost vertical yellow beam in Figure 12.

Figure 12: LH stub wing side with dummy landing gear (yellow) and hydraulic actuator installed, courtesy of INCAS & AVIATEST.

For the landing gear load cases this specimen was used to verify the ultimate strength of the stub wing for loads caused by hard landing. This was one of the few tests where UL load was applied. Even after UL was reached the final step was to increase the load till rupture in order to determine the absolute limit of the structure.

Figure 13 shows a detail of the collapsed area of the stub wing test in the transition between stub-wing and fuselage in the proximity of the main frame where boundary conditions have been applied. The failure mode was a combined failure of several items collapsing sequentially.

Figure 13: Stub wing after final test with rupture beyond ultimate load. View is showing transition stub wing to fuselage with rupture close to the boundary

condition (lower end of the figures), courtesy of INCAS & AVIATEST.

During all tests instrumentation composing displacement transducers and strain gauges were installed and compared to the predictions. All testing presented in this chapter was defined and accompanied by INCAS in Bucharest and performed at AVIATEST in Riga as qualified laboratory (Ref. 13).

5.3. Testing of the upper deck area

Set-up description:

All new design principles in the upper deck as described in chapter 5.1 are subjected to testing in this sub-component test. The main challenge of this test campaign was the very limited space available in the upper-deck area. Due to the attachment of the upper wings this area is even more congested with structural items. The MGB, wings, anti-torque device and MGB struts act simultaneously on this area of the fuselage. Consequently, even the space for a dummy MGB as main loading device is very limited.

It turned out that a complete test with simultaneous actuation at all major interface points was too complex. There are 12 main load introduction points with load vectors in different orientations in almost any combination of magnitude and direction, see Figure 14 which shows the load introduction points in the upper deck area. Besides these main load introduction points, in the real structure the adjacent structural items like intermediate structure or front fuselage contribute to the loading of this area (remember the complex deformation shown in Figure 7).

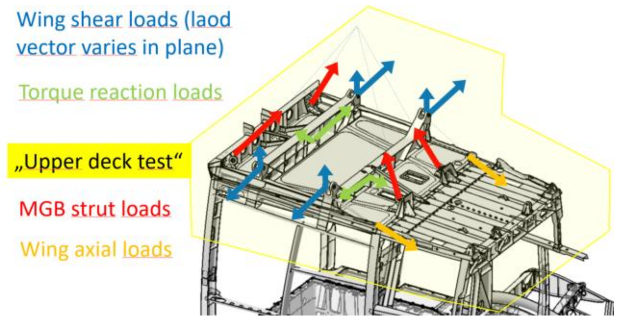

Figure 14: Principal sketch of the main load introduction points of the RACER's upper deck area.

Studies based upon the global finite element model proved that the differences in testing of the new design principles in a full model and in the component test are very small and are embedded properly in the set-up so that boundary effects can be neglected. In this context the proper elasticities of the upper deck assembly ensure a realistic load path when loading the individual elements. The secondary effect of the complete interaction of all loaded parts for many of the load cases was covered by FE-studies of the test set-up. With this FE-model correlations between the loading conditions in the global helicopter model and the isolated item were performed.

For the selected load cases the FE predicted deformations and resulting stress levels have been "tuned" by artificial scaling factors which were applied on the individual load components in order to achieve a realistic deformation and stress level in the structural members subjected to test. This is shown as an example in Figure 15. In the upper area of this figure the stresses and deformations of the cross beams are shown when the item is loaded in the global helicopter model (GFEM) for one specific load case. The lower part of the figure shows the same item with a simulated and "tuned" loading with load enhancement factors and adapted boundary conditions.

It becomes visible from this figure that the elastic deformation as well as the stress distribution in the part is very similar and thus a valid representation of the loaded part is achieved.

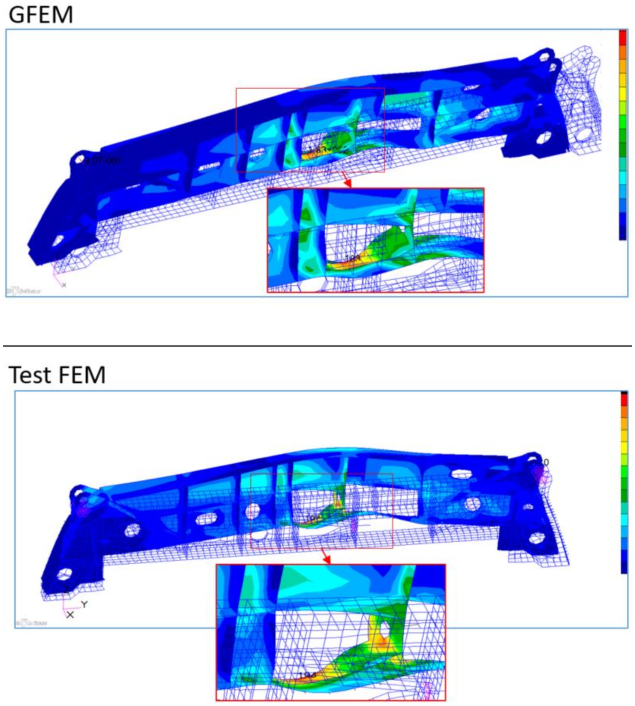

Figure 15: Comparison of the loading of a cross-beam in the upper deck showing deformation and stress distribution for one load case (exaggerated). Upper: Global model, Lower: Isolated test specimen after tuning.

This "tuning" procedure of achieving a good similarity of loading, elastic deformation, and stress distribution between test sample and the complete vehicle real structure was performed for all structural members which are in the main focus of the test. Although the main interest was to test the new design principals, all other main structural items in this area such as torque panel or MGB brackets have been loaded up to limit load as well. This was in order to demonstrate proof strength not only for the new structural parts but for all items in the MGB attachment zone in general.

As mentioned before, in the real vehicle all adjacent parts are loaded simultaneously with changing and complex interaction. In the test a subset of these loads is applied at selected major interface points only. This is a simplification by skipping superposition with fluxes passing through this area of the structure as for example forces from the tail. So the main task in preparation of the test campaign was to find the best approximation of the loading on each single part under real flight conditions. As a result a simple MGB dummy with *separated load components* was designed, see Figure 16. It is a simple device offering direct load paths with parallel or perpendicular individual load vectors in order to achieve a combination of bending moments, forces and torque of each *separate item* in the real structure. With this design individual interface loads on the components can be controlled by *direct application of interface loads* (onwards denominated as "direct control" of interface loads).

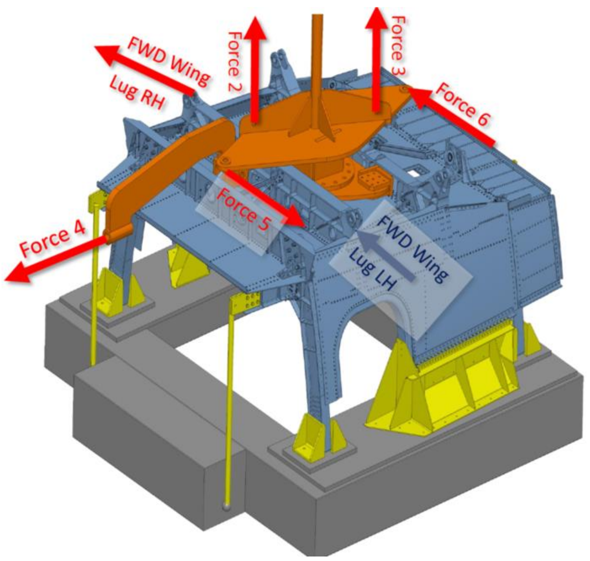

Figure 16: MGB dummy (in orange colour) with capability of applying loads to individual main structural components in the upper deck in "direct control" manner.

This strategy of "direct control" of interface loads is different from the strategy to simulate the loading on the complete upper deck test article as performed in other Airbus Helicopter programs in the past. For other programs large dummy MGB structures were designed for applying the resultant forces and moments of the main rotor. These almost rigid MGB dummies distribute the resulting main rotor forces and moments to the interface points *simultaneously* according to the elasticity of the upper deck arrangement. In this type of set-up a dedicated "control" of the single forces on each item is not possible as an increase or decrease of the *resulting applied load* is impacting all other interfaces at the same time (denominated in this paper as "in-direct control" of interface loads).

The main difference between "direct and "in-direct" control of interface loads is the impact from the elasticity of the whole article and the load distribution this creates in the individual structural members. In the "in-direct control" principle the elasticity of the upper deck arrangement is effective immediately as the applied force distributes according to the total upper deck stiffness. Whereas for the "direct control" strategy, chosen for the RACER, the elasticity is determined by the boundary conditions only, but not as superposition of simultaneous loading. Thus the effect of simultaneous loading has to be covered by analysis as "tuning" factors" for the load magnitudes (see above). In order to validate the real elastic effect the GFEM validation test, at top of the test pyramid, was performed (see §4).

Test execution:

For all the upper deck tests the set-up (means: boundaries) and load application (means: position and magnitudes) was adapted individually for each test or component respectively. As example Figure 17 shows the set-up of one of the upper deck tests focussing on the LL application of the front crossbeam.

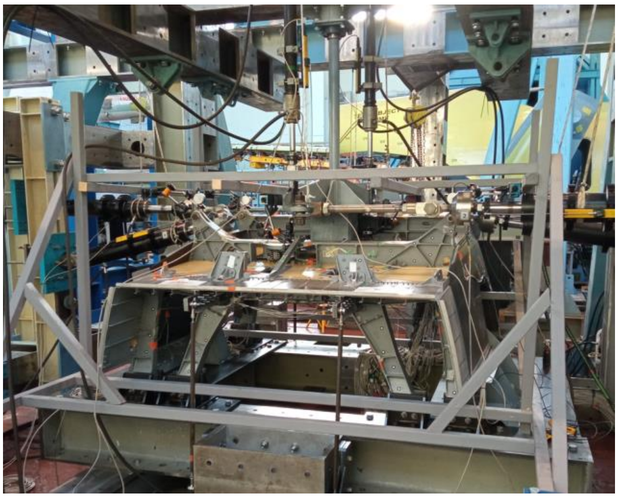

Figure 17: Set-up of the front cross beam test in the test campaign.

In addition to the comparatively complex load application for the upper deck cross-beams, several tests were performed with one-directional axial loading on the MGB brackets, x-struts, or wing lugs. This was a simple tests of the respective interfaces with one cylinder only, see as example the set-up shown for the front MGB bracket in Figure 18.

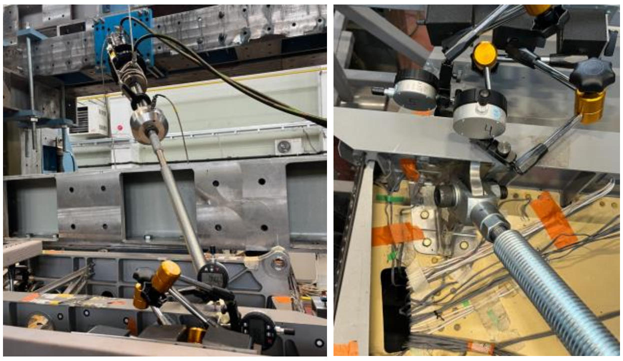

Figure 18: Test of the MGB bracket.

Apart from the strength driven tests, additional tests have been performed in order to check the stiffness criterion which is to be fulfilled for the cross-beams as they support the upper wings with the lateral drive shaft inside (see Ref. 3). At the upper wing to fuselage junction a soft coupling is located with limited angular deflection capability. The cross-beams ensure that the limits of this coupling are not exceeded. These stiffness tests were carried out with unitary loads in lateral direction by loading both opposite wing lugs at the same time in order to create a symmetric loading condition.

All testing described in this sub-chapter as well was defined and accompanied by INCAS in Bucharest and performed at AVIATEST in Riga as qualified laboratory.

5.4. Testing of the RACER's wings

The wing function is to provide aerodynamic lift, trim by virtue of rotary actuated flaps, house the lateral drive shaft, and to support the lateral rotor gearbox (LRGB). Together the left and right rotors provide anti-torque to the main rotor making the supporting wing load paths critical to continued safe flight and landing. Therefore these loadpaths must be substantiated according to the applicable paragraphs of CS-29. Of particular importance is the LRGB attachment structure (cradle) which is a single piece cast titanium component. With its complex loading and geometry the distribution of stress concentrations leading to initiation of fatigue damage are difficult to predict, even with finite element modelling. The upper wing houses the lateral rotor drive line (LDL) thereby imposing strict deflection requirements to maintain radial clearance between the LDL and internal wing structure. In addition, there are global wing deflection requirements to keep the drive line universal couplings within operational limits, see Ref. 3.

The means of compliance for the regulatory and performance requirements is analysis validated by test. The design analysis is based on a finite element model representing the wing primary load paths and aerodynamic surfaces. The model was subjected to static loading simulating a range of flight and emergency landing conditions. Stress, strains and reaction forces were recovered.

To validate the design analysis and structural ground test, the subject of this article, was conducted with the following objectives:

1. Substantiation of proof of strength under Limit Load.
2. Substantiation of fatigue endurance.
3. Substantiation of LDL clearance and global wing deflections.
4. Validation of the internal loads distribution in the linear finite element model (FEM).

For cost and schedule reasons all testing was completed on a single test article and the sequence of testing was arranged in order of ascending risk for specimen preservation.

The design and manufacture of the test article is identical to the flight article with the exception of non-primary structure such as flaps and fairings which were excluded. The wing was mounted to a steel test fixture, considered rigid, with representative fuselage interfaces, see Figure *19* and Figure *20*. Three linear actuators were mounted to both upper and lower wings to simulate aerodynamic loading.

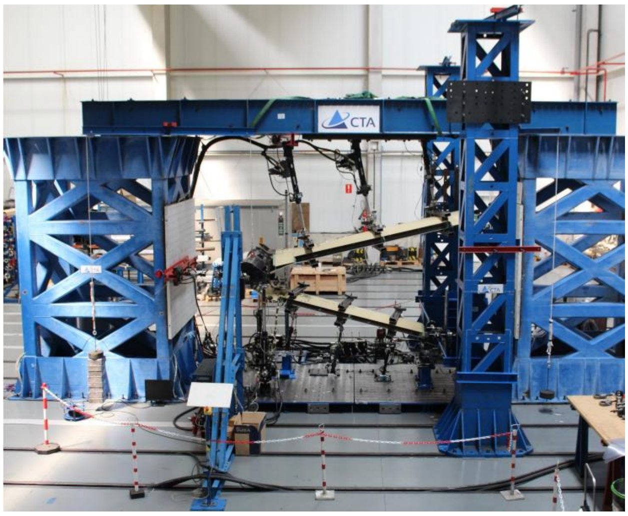

Figure 19: Test rig general layout

'Two bridge' load cells measured force reactions at the fuselage (test rig) interface.

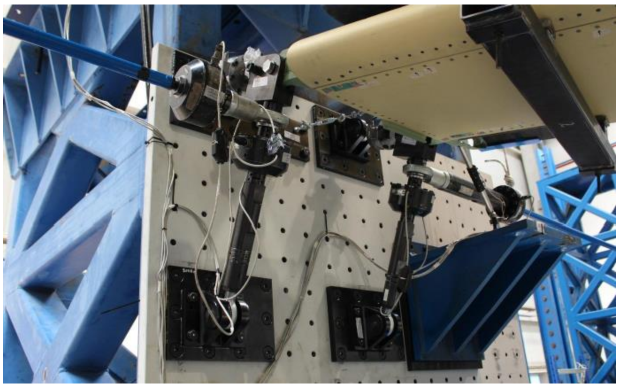
Figure 20: Upper wing fixation points representative of the fuselage interface

A replica gear box was manufactured from steel and mounted to the Cradle with representative interfaces which is shown as a black cylinder in Figure *21*. Linear actuators were mounted to the replica gear box to simulate thrust, gearbox torsion about the chordwise axis and LDL torsion about the spanwise axis.


Figure 21: Front and rear views of the replica gearbox.

A total of 5 struts, designed to react thrust and LRGB torque loads, were instrumented and calibrated to measure force reactions. Strains were measured with a combination of linear and rosette gauges positioned at sites of interest across the Wings and Cradle.

Displacements were measured with Linear Variable Displacement Transducers (LVDTs) positioned at each actuator.

A tension wire was installed in the upper wing to represent the theoretical axis of the LDL. At the inboard end the wire was attached to the test rig at the inboard universal coupling position. The outboard end was attached at the outboard universal coupling position to a wooden plate inserted into the Cradle opening where the LDL passes through. This arrangement is shown in Figure 22 and Figure 23.

Figure 22: Test Section view of upper wing showing LDL

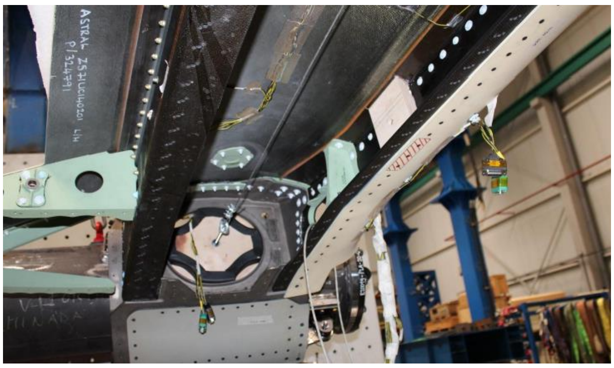
Figure 23: Tension wire representing the LDL mounted to a wooden plate in the Cradle opening

(view of upper wing from below with lower cover removed).

A transducer was used to measure the upper wing deflection relative to the un-deflected tension wire (Figure 24).

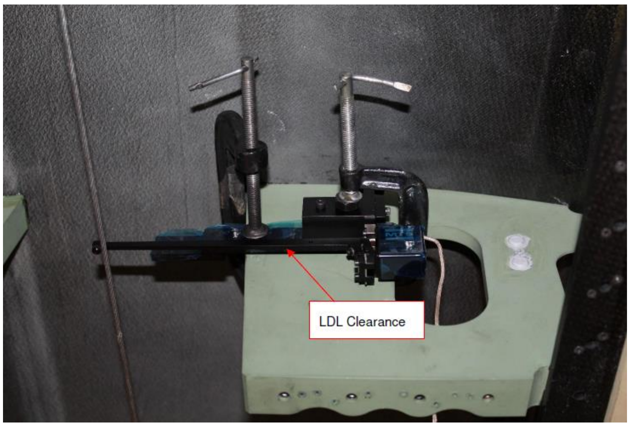

Figure 24. LDL clearance transducer.

Figure 25 shows a schematic of the LDL in the upper wing in a front view.

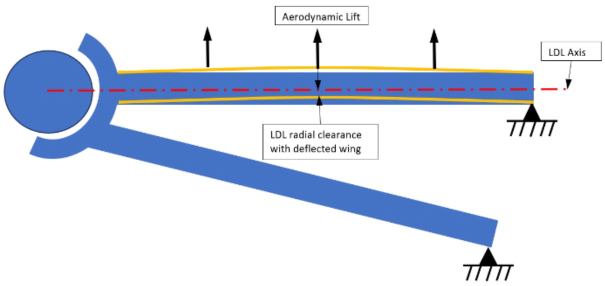

Figure 25: Schematic showing LDL axis and its radial clearance to the wing structure.

A FEM was created to represent the test set up with the applied loading modelled as discrete source inputs which is a simplification of the more complex aerodynamic and LRGB loads applied in the design FEM. This test FEM, including the load application points, is shown in Figure 26. Test load correction factors were then calculated to ensure the load distribution at the wing to fuselage (test rig) interfaces in the test FEM matched the design FEM, thus confirming the test set up as an acceptable representation. The test rig and fuselage are assumed rigid in the respective test and design FEMs.

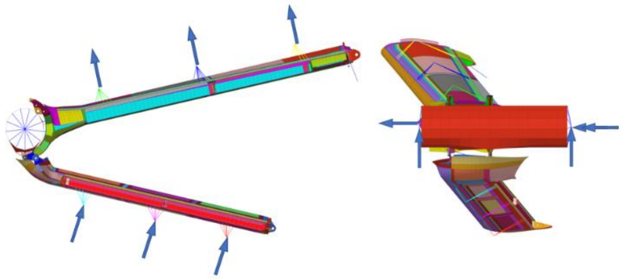

Figure 26: Test FEM with applied loading points.

The first tests performed were low load 'unit' tests to validate the internal load distribution in the test FEM. Each discrete load introduction point was activated in turn and the reactions measured at the fuselage interfaces. The acceptance criteria is a test-to-prediction correlation of ±10%, measured at the fuselage interfaces and other gauged locations. However it was observed that the applied unit loads were insufficient to excite a response above the non-linear range due to structural settlement. Therefore limit load test results were also used for the FEM validation.

Limit load tests were performed for a total of 7 different flight cases, each targeting a different LRGB to Cradle or wing to fuselage interface. Doing so ensured each interface considered critical to continued safe flight and landing, was subjected to 100% limit load at least once and that the global structure was sufficiently exercised.

The deflection test for radial clearance to the LDL was performed with maximum aerodynamic loads in the upper wing giving it its maximum deflected shape.

For the fatigue test the test article was subjected to a spectrum comprising 8 segments of blocked monotonic cycles (R=0.1), representative of a typical mission. The fatigue test configuration was unchanged from the limit load tests and each load cycle comprised a combination of aerodynamic and LRGB input loading. Applied cycles totaling the target life were achieved over 10 tests, each accumulating 10% of the total cycles. Each test was accelerated so that it could be completed within 24 hours. Between each block a low level static reference case was applied to check the specimen status.

6. TEST RESULTS

The upper level tests of the test pyramid presented in this paper served six major purposes:

1) to show LL capability,

2) to show no detrimental or permanent deformation at LL with small hysteresis,
3) to demonstrate the minimum required stiffness is achieved in the upper deck,
4) to prove the clearance of the LDL in the upper wing,
5) to demonstrate that the simplified fatigue campaign does not initiate crack at the wing interfaces,
6) to validate the analysis models at GFEM level.

Globally, all test goals have been met. Apart from some spots all measured strains showed a linear behavior up to LL. Figure 27 shows a typical force-strain plot of selected strain gauges in the stub-wing test campaign. It can be seen that the predictions (plotted as dashed lines) are well met by the test results (continuous line) within a precision of ±10% which is considered to be the acceptable range of precision. Where there were larger mismatches the gauges were typically placed in zones of high stress gradients where small differences in position lead to a significant change in the strain level. Gauges placed in zones of very small strain also meant that any relative mistakes in gauging, amplification or resolution al lead to a large mismatch.

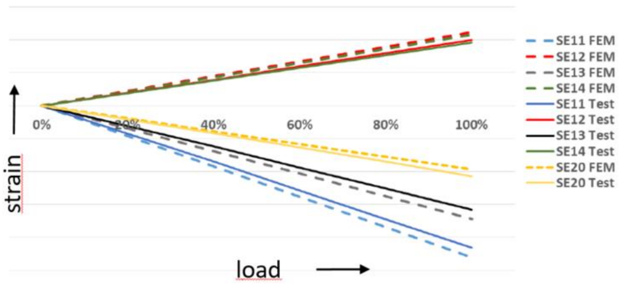

Figure 27: Force-strain plot of selected strain gauges in the stub-wing test campaign (FEM: dashed line, test: solid line).

All tests up to LL successfully demonstrated no detrimental permanent deformation. Moreover, the almost linear force-displacement curves showed a low hysteresis, see as example Figure 28. The slight non-linearities are caused by gaps in the load path as well as by geometric non-linear effects caused by lever arm changes during the load application.

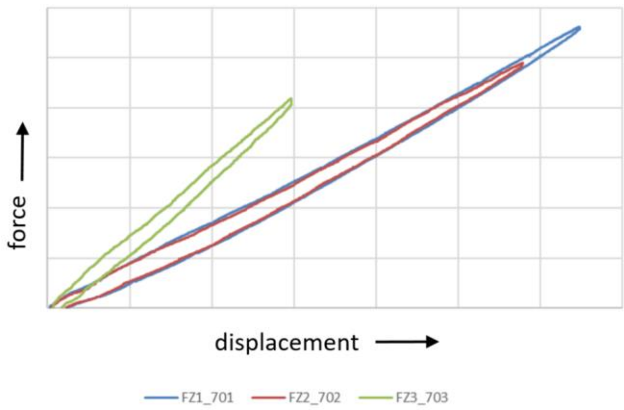

Figure 28: Force-displacement plot of load cells measured during the maximum deflection test of the wing.

In the wing tests the results proved that the fuselage interface reactions were within ±10% of the analytical prediction with only minor exceptions. All strain gauges with a significant signal magnitude showed a correlation within ±10%. Instances exceeding ±10% were for low load conditions. Each of the 7 limit test cases proved acceptable strength capability without failure and without permanent set within the metallic structure. Interval and final DVI inspections confirmed no damage to metallic or composite structure.

The fatigue tests were done to prove no fatigue failure will happen in structure before the design service goal of the helicopter with a scatter factor of 3. After 30% of the total cycles the wing access panels were removed for SDI and DVI inspections. In addition, the critical pin at the LRGB to Cradle interfaces was removed and inspected with LFEC. The target life was achieved without failure or reportable damage.

The outcome of the test proved the wing meets all regulatory and deflection requirements and all anomalies can be justified by analysis or engineering judgment.

The test campaign proved that the stiffness criteria are met in the upper deck (cross-beams for interconnection of the wings). It was demonstrated that the real stiffness in the upper deck actually exceeds the minimum required calculated stiffness. The wing stiffness test showed that the minimum radial clearance requirement was met, demonstrating acceptable wing stiffness.

The final evaluation of the GFEM validation test is not finished completely. With the exception of one, all tests in the pyramid have been performed at the time or writing. During the execution of the tests no un-expected behavior was recorded or recognized.

Detailed test results and interpretation remain part of the PtF documentation.

7. CONCLUDING REMARKS

1. The test campaign of the major structural components ended in first quarter 2023. No safety relevant findings recorded in the tests. LL capability was shown for all tested structural components. No crack initiation recorded after the fatigue test campaign and all stiffness criteria are met.
2. The correlation between GFEM and the real structure is correlating well and thus the tests have proven the analysis models are representative. This validated the strategy to split the tests up into a several separated sub-component tests and thus verified the decision not to build a full-scale vehicle for testing.
3. With this strategy a rather simple but thorough test campaign was conducted for the RACER which supported the verification of the analysis results, the proof of structural strength, and the applicability of the methods and tools used during the development of the RACER's formula.

Author contact:

Martin Blacha: martin.blacha@airbus.com

Peter Burden: peter.burden@hambleaero.com

8. ACKNOWLEDGMENTS

The authors would like to acknowledge the European Union for funding of the activities of the RACER development in the Clean Sky 2 program and all partners involved in the RACER project supporting the activities in all fields.

Specifically the authors acknowledge the Romanian Institute of Aeronautics (INCAS) for the supporting this paper as part of their work-package in the RACER.

Special thanks as well to AVIATEST in Latvia who conducted the tests on the fuselage and to CTA in Vitoria, Spain for their support and expertise during the wing test.

9. REFERENCES

1. European Union Aviation Safety Agency (EASA), "Certification specification and acceptable means of compliance and guidance material for large rotorcraft CS-29," Cologne, Germany, 2021.
2. Advisory circular of the Federal Aviation Administration (FAA), CS29, AC20-107B.
3. Blacha, M., Garcia-Rios, A., Schelcher, M., and Cabrit, P., "Clean Sky 2: Exploring new rotorcraft high speed configurations" European Rotorcraft Forum 43rd Annual Forum Proceedings, Milan, September 2017.
4. Blacha, M., Fink, A., Miles, R., Jimenez, J-M:, "The RACER: Manufacturing and Testing", European Rotorcraft Forum 47th Annual Forum Proceedings, Glasgow, UK, September 2021.
5. Stokkermans, T., Voskuijl, M., Veldhuis, L., Soermarwoto, B., Fukari, R., Eglin, P. "Aerodynamic installation effects of lateral rotors on a novel compound helicopter configuration", 74th AHS International Annual Forum & Technology Display, Phoenix, Arizona, USA, May 14-17, 2018.
6. Zenker, T., Jennemann, F., and Wegmann, M. 2020. Automated Fiber Placement based manufacturing of carbon fiber reinforced sandwich helicopter side shells. In 1st Aerospace Europe Conference AEC2020.
7. Salah el Din, I., Lineard, C., Huot, R., Fukari, R. "RACER high speed demonstrator: tail unit vertical fin aerodynamic design", Vertical Flight Society`s 75th Annual Forum & Technology Display, Phoenix, Arizona, USA, May 14-17, 2018.
8. Blacha, M., Fink, A., Eglin, P., and Cabrit, P., "Clean Sky 2: Exploring new rotorcraft high speed configurations" European Rotorcraft Forum 43rd Annual Forum Proceedings, Milan, September 2017.
9. Huot, R., Eglin, P. "Flight Mechanics of the RACER compound H/C". Vertical Flight Society's 76th Annual Forum & Technology Display, Virginia Beach, Virginia, USA, Oct. 6-8, 2020.
10. Cander, D., Geneix, J., Depouhon, P. "Advanced concept of drive shaft system for hybrid high speed helicopter", 45th ERF European Rotorcraft Forum, Warsaw, Poland, 17-20 September, 2019.
11. Fink, A. et al. European Patent EP 2690011 B1, "Compound helicopter".
12. Jimenez, J-M., "DISRUPTIVE AND EFFICIENT REAR FUSELAGE FOR DUAL USE HIGH SPEED ROTARY WING PLATFORMS", Joint

10th EUCASS – 9th CEAS Conference, Aerospace Europe Conference, Lausanne, Switzerland, July 2023.

13. N.N., “Aviatest - Full-scale static, dynamic and fatigue testing of airplanes, helicopters and other aircrafts structural components”, 33rd European Rotorcraft Forum, Kazan, Russia, 2007.